

Superfluid density and microwave conductivity of FeSe superconductor: ultra-long-lived quasiparticles and extended s-wave energy gap

Meng Li,¹ N. R. Lee-Hone,² Shun Chi,¹ Ruixing Liang,^{1,3}
W. N. Hardy,^{1,3} D. A. Bonn,^{1,3} E. Girt,² and D. M. Broun^{2,3}

¹*Department of Physics and Astronomy, University of British Columbia, Vancouver, BC, V6T 1Z1, Canada*

²*Department of Physics, Simon Fraser University, Burnaby, BC, V5A 1S6, Canada*

³*Canadian Institute for Advanced Research, Toronto, Ontario, M5S 1Z8, Canada*

FeSe is an iron-based superconductor of immense current interest due to the large enhancements of T_c that occur when it is pressurized or grown as a single layer on an insulating substrate. Here we report precision measurements of its superconducting electrodynamics, at frequencies of 202 and 658 MHz and at temperatures down to 0.1 K. The quasiparticle conductivity reveals a rapid collapse in scattering on entering the superconducting state that is strongly reminiscent of unconventional superconductors such as cuprates, organics and the heavy fermion material CeCoIn₅. At the lowest temperatures the quasiparticle mean free path exceeds 50 μm , a record for a compound superconductor. From the superfluid response we confirm the importance of multiband superconductivity and reveal strong evidence for a finite energy-gap minimum.

A recurring theme in correlated electron research is the sensitivity of such materials to small perturbations, which, when applied, can tune the material through a range of distinct electronic ground states.^{1–6} At the heart of this behaviour is a delicate balance between kinetic energy and potential energy, with kinetic energy favouring delocalized electrons and potential energy promoting various types of electronic order. This balance can be tipped in one direction or the other by the application of magnetic field⁷ and hydrostatic pressure,⁸ and by making small changes in chemical composition.^{9,10} In the iron-based superconductor FeSe, the first indication of this sensitivity occurs at around 90 K when the material changes from tetragonal to orthorhombic as it enters a nematic phase,^{11,12} lowering rotational symmetry without breaking translational symmetry. At lower temperatures FeSe becomes a superconductor, at $T_c \approx 9$ K under ambient conditions,¹³ with T_c rapidly increasing by a factor of 4 under hydrostatic pressure.¹⁴ Even more dramatic enhancements occur in single-layer FeSe grown on insulating and semi-insulating substrates such as SrTiO₃, with reported values of T_c up to 100 K.^{15–18} A major effort is now underway to understand this fascinating new example of high temperature superconductivity.

FeSe is one of the simplest iron-based materials, superconducting at its stoichiometric composition and available as high quality single crystals grown using vapour transport methods.^{19,20} A crucial question is to understand what the bulk, ambient superconductor is holding in reserve, that it can respond so strongly when pressurized²¹ or placed in contact with a substrate.²² Central to addressing this issue is the identification of the superconducting gap structure and, ultimately, the pairing glue.^{21–26} On the question of gap structure, a number of measurements emphasize the importance of multiband superconductivity,^{27–32} but differ on whether or not the energy gap has nodes. The main evidence for nodes appears in a combined study³⁰ that reports large residual thermal conductivity and power-law pen-

etration depth, $\lambda(T)$, although these conclusions are by no means universally agreed on.^{32–34} A number of scanning tunnelling microscopy (STM) studies show evidence of V-shaped tunneling spectra,^{30,35} but the picture here is also complicated. Some STM studies report features that look more like finite gaps,^{31,36} and there can be a complicated interplay with twin boundaries.³⁶ In addition, within experimental uncertainty, all STM studies appear to observe zero conductance at zero bias, something that can only occur if there is a single-particle gap at least three times the measurement temperature. This on its own would imply a finite gap minimum in the range $\Delta_{\text{min}}/k_B \approx 1.2$ to 4.5 K. Also weighing in in favour of a finite gap minimum are a number of bulk probes including heat capacity,^{28,31} thermal conductivity,³⁴ μSR ,³⁷ lower critical field³³ and penetration depth.³²

In the work reported here we use precision low temperature measurements of the electrodynamic response of FeSe to shed further light on its gap structure and superconducting charge dynamics, in the process revealing extremely long-lived quasiparticles, a testament to the high degree of crystalline order that is possible in this intriguing material.

Results

In the low frequency limit the electrodynamics of a superconductor are dominated by the superfluid response, giving rise to perfect dc conductivity. Far from being a quiescent state, Cooper pairs are continually being broken apart into quasiparticle excitations then reforming in a phase-coherent manner — such scattering does not degrade a steady current and is important in establishing the equilibrium superfluid density.³⁸ In order to study the electrodynamic response of the quasiparticles, higher frequencies are needed, ideally comparable to the quasiparticle relaxation rate. Because the superfluid has finite inertia, a high frequency supercurrent is accompanied by an electric field, which in turn couples to the quasiparticle excitations and gives rise to

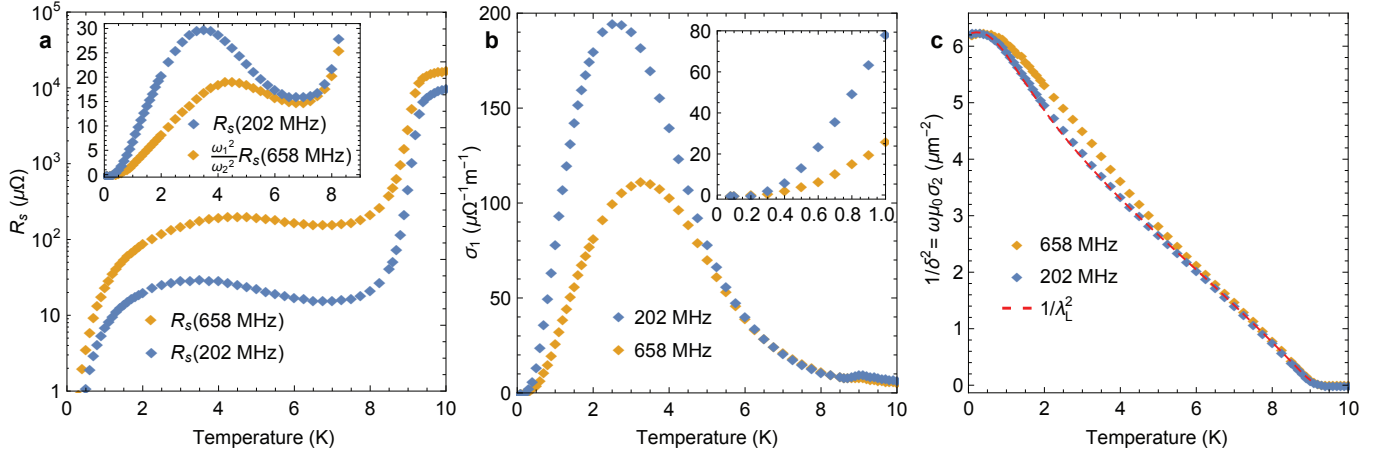


FIG. 1. **Electrodynamical response of FeSe superconductor at 202 and 658 MHz.** (a) Surface resistance of FeSe with R_s on a logarithmic scale. Inset: zoomed-in view of R_s in the superconducting state on a linear scale, with the expected ω^2 frequency dependence of R_s scaled out at the higher frequency. (b) Real part of the quasiparticle conductivity, $\sigma_1(T)$. Inset: zoomed-in view showing the freeze-out of conductivity at low temperatures. (c) Frequency dependent superfluid fluid density, $1/\delta^2 \equiv \omega\mu_0\sigma_2$. The dashed line shows the London superfluid density, $1/\lambda_L^2 \equiv 1/\delta^2(\omega \rightarrow 0)$.

a dissipative response. This results in power absorption that increases as ω^2 and is directly proportional to the real part of the quasiparticle conductivity, σ_1 .

Surface impedance. The experimentally accessible quantity is the surface impedance, $Z_s = R_s + iX_s$, with $R_s \approx \frac{1}{2}\omega^2\mu_0^2\lambda^3\sigma_1$ and $X_s \approx \omega\mu_0\lambda$. As we will show below the quasiparticle lifetimes in FeSe are extraordinarily long for a compound superconductor. Experimentally, this means that the GHz-frequency resonators typically used in this type of measurement are too fast, not allowing the quasiparticles sufficient time to relax during the measurement period. That said, surface resistance measurements face significant difficulties at lower frequencies and are rarely attempted:³⁹ R_s falls off as ω^2 and the characteristic size of resonators increases like $1/\omega$, making a mm-sized single crystal a negligible perturbation inside a large resonator volume. Our solution has been to employ a special self-resonant coil, of diameter 4 mm and length 10 mm, wound from superconducting Nb wire and operating at $\omega_1/2\pi = 202$ MHz and $\omega_2/2\pi = 658$ MHz, with empty-coil quality factors of several hundred thousand. Such a resonator has sufficient sensitivity to resolve both the superfluid and quasiparticle response of a mm-sized crystal of FeSe.

Figure 1a shows surface resistance data for FeSe at the two frequencies. There is a sharp superconducting transition at $T_c = 9.1$ K, indicative of a homogeneous sample. Surface resistance drops quickly as Meissner screening currents take over from the normal-state skin effect, with $R_s(T)$ reaching a minimum at $T \approx 7$ K. Below this temperature the surface resistance rises again, with a peak that moves to lower temperature with decreasing frequency. At the lowest temperatures R_s falls again, decreasing into the $\mu\Omega$ range. The nonmonotonic temperature dependence of R_s has

been observed in only one other material system — ultrahigh purity $\text{YBa}_2\text{Cu}_3\text{O}_{6+x}$ — and is immediately indicative of a system with rapidly collapsing scattering and extremely long-lived quasiparticles.^{40–43} The main differences between FeSe and $\text{YBa}_2\text{Cu}_3\text{O}_{6+x}$ are twofold: the details of the freeze-out of $R_s(T)$ at low temperatures suggest a finite energy gap in FeSe, instead of the symmetry-protected d -wave nodes in $\text{YBa}_2\text{Cu}_3\text{O}_{6+x}$;^{44,45} and in FeSe the nonmonotonic $R_s(T)$ appears only below about 1 GHz, as compared to about 70 GHz in $\text{YBa}_2\text{Cu}_3\text{O}_{6.993}$.^{42,43} This on its own suggests that quasiparticles lifetimes are unusually long in FeSe.

Microwave conductivity. From the surface impedance we obtain the high frequency conductivity $\sigma = \sigma_1 - i\sigma_2$. The real part of the conductivity is plotted in Fig. 1b for the two measurement frequencies and shows more clearly the underlying quasiparticle dynamics that are responsible for the nonmonotonic form of $R_s(T)$. On cooling through T_c , $\sigma_1(T)$ starts to rise. In this temperature range σ_1 shows no appreciable frequency dependence, consistent with a quasiparticle relaxation rate that is much larger than the measurement frequencies. On further decreasing temperature $\sigma_1(T)$ rises rapidly, eventually peaking at around a third of T_c , at a value 40 times higher than $\sigma_1(T_c)$ in the case of the 202 MHz data. As well as in the $\text{YBa}_2\text{Cu}_3\text{O}_{6+x}$ system^{40,42,43,46} qualitatively similar behaviour is observed in the heavy fermion superconductor CeCoIn_5 ,^{38,47} and the organic superconductor $\kappa\text{-(BEDT-TTF)}_2\text{Cu[N(CN)}_2\text{]Br}$,⁴⁸ although only in Ortho-I $\text{YBa}_2\text{Cu}_3\text{O}_{6.993}$ is the enhancement as dramatic. In all cases the physics is the same — on passing through T_c there is a sudden collapse in quasiparticle scattering that vastly outpaces the steadier condensation of quasiparticles into the

superfluid condensate. Consistent with this conclusion σ_1 develops substantial frequency dependence below $T_c/2$, indicating that the quasiparticle relaxation rate is becoming comparable to the measurement frequency — in the case of FeSe, a relaxation rate in the sub-GHz range.

Superfluid density. The imaginary part of the conductivity is dominated by the superfluid term, $\sigma_s = 1/i\omega\mu_0\lambda_L^2$, where λ_L is the London penetration depth. We plot the frequency-dependent superfluid density, $1/\delta(\omega)^2 \equiv \omega\mu_0\sigma_2(\omega)$, in Fig. 1c. There is some frequency dependence in the lower part of the temperature range, consistent with the presence of slowly relaxing quasiparticles below $T_c/2$ that eventually freeze out at the lowest temperatures. Fits to a generalized two-fluid model (see Methods) are used to extrapolate $\omega\mu_0\sigma_2(\omega)$ to the static limit and obtain the London superfluid density, $1/\lambda_L^2$. The superfluid density shows a strong, approximately linear temperature dependence over most of the temperature range, with upwards curvature in $1/\lambda_L^2(T)$ at around $T_c/3$, which we will discuss below in the context of multiband superconductivity. At the lowest temperatures there is a substantial flattening of $1/\lambda_L^2(T)$, similar to that seen in $R_s(T)$ and $\sigma_1(T)$, that we will show is evidence of small but finite gap minima in one of the bands. Broadly similar behaviour in $1/\lambda_L^2(T)$ has very recently been reported in Ref. 32.

Discussion

To gain further insight into the superconducting charge dynamics we have fit a generalized two-fluid model (see Methods) to the complex conductivity: at each temperature this gives the average quasiparticle relaxation rate, Γ , and the London superfluid density. The relaxation rate is plotted in Fig. 2. As expected from the qualitative behaviour of $R_s(\omega, T)$ and $\sigma_1(\omega, T)$ there is a rapid collapse in $\Gamma(T)$ on cooling into the superconducting state, which in the context of the cuprates, organics and CeCoIn₅ is interpreted as a strong indication that the fluctuations responsible for inelastic scattering are electronic in origin and are gapped by the onset of superconductivity. Another factor that is relevant to the suppression of $\Gamma(T)$ in these systems is the importance of Umklapp processes in relaxing electrical currents^{49,50} — as we will discuss later, energy conservation in Umklapp events becomes difficult to satisfy in multiband superconductors with anisotropic gap. Below 2.5 K $\Gamma(T)$ locks into a linear temperature dependence. Such behaviour is reminiscent of cuprate superconductors in the Born-scattering limit,^{51–54} where the linear temperature dependence of Γ reflects the linear-in-energy density of states (DOS) of the *d*-wave quasiparticles. We will argue below that the energy gap in FeSe has an extended *s*-wave form, with deep gap-minima — such a state is accompanied by a linear DOS at energies immediately above the gap minimum and possibly leads to

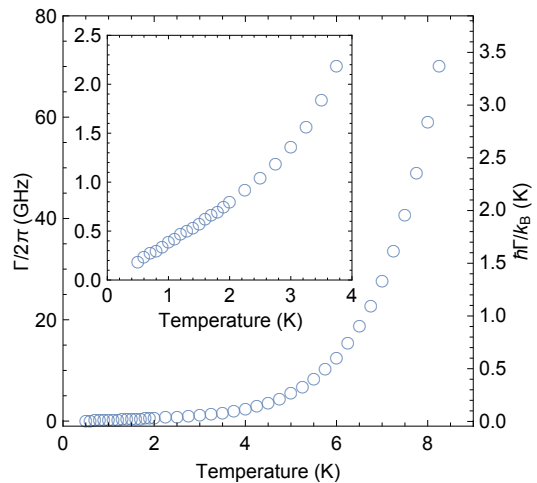


FIG. 2. Quasiparticle relaxation dynamics. The quasiparticle relaxation rate, $\Gamma(T)$, is obtained from the fitting to conductivity with a modified Drude model. For reference, the normal-state relaxation rate is approximately 135 GHz at 12 K. Inset: low temperature zoom, revealing an approximately linear temperature dependence of Γ between $T = 0.5$ and 2.5 K.

$\Gamma(T) \propto T$ in the intermediate temperature range. Below $T = 0.5$ K, there is insufficient quasiparticle conductivity to carry out accurate fits to the two-fluid model, so Γ is not plotted in this range. At the lowest temperatures the scattering rate is $\Gamma_{\min}/2\pi \approx 200$ MHz, corresponding to $\hbar\Gamma_{\min}/k_B \approx 10$ mK in temperature units. Using a value of $v_F \approx 7 \times 10^4$ m/s for the Fermi velocity,¹² the quasiparticle mean free path is $\ell_0 = v_F/\Gamma_{\min} \approx 55$ μm . This is the largest value we are aware of for a compound superconductor and is 5 times larger than that of the best YBa₂Cu₃O_{6.52} crystals, where the low temperature scattering rate reaches $\Gamma/2\pi \approx 3.3$ GHz.⁵³ On the experimental side, we emphasize that this result is on a firm footing, as our lowest measurement frequency is of the same order as $\Gamma_{\min}/2\pi$. Although ℓ_0 is larger than almost any other length scale in our sample, non-local effects are likely suppressed by four different considerations: the larger-than-normal in-plane penetration depth in FeSe^{30,33,37} ($\lambda_0 \approx 400$ to 500 nm); the quasi-2D electronic structure,^{12,55–57} which, in our experimental geometry, forces quasiparticles to propagate at low angles to the sample surface; the vanishing of quasiparticle group velocity near the gap minima; and the diffusive nature of small-angle scattering in a superconductor with anisotropic gap.⁵⁸ The last two points work together to make the distance travelled by the quasiparticle wavepacket between large-angle scattering events much smaller than the apparent mean free path. Even taking into account the significant enhancements of electrical mean free path due to these effects, the inferred value of ℓ_0 is remarkable and suggests that FeSe may provide a novel testing ground for exploring hydrodynamic effects^{59,60} in superconducting transport.

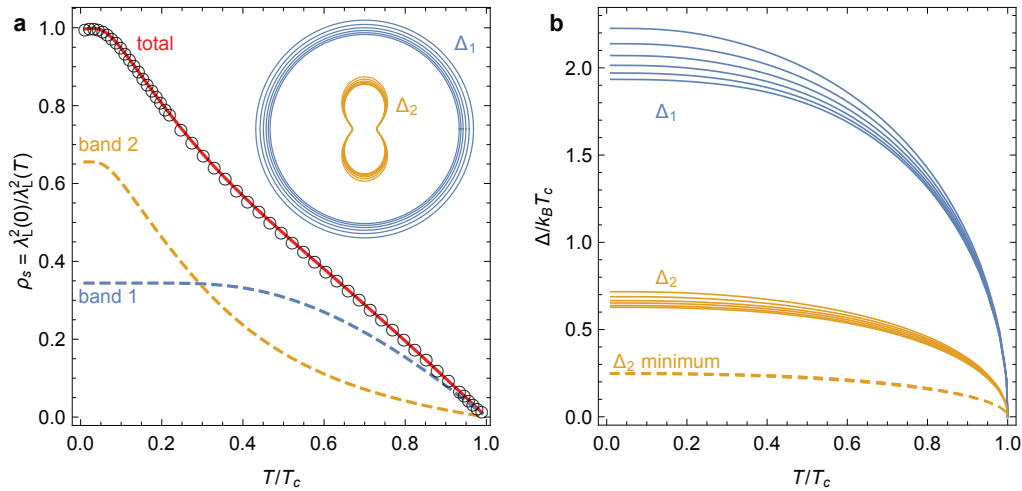


FIG. 3. **Superfluid density in a two-band extended s-wave model.** (a) Superfluid density is calculated using a two-band extended s-wave model and fit to the London superfluid density, $1/\lambda_L^2(T)$. Inset: A polar plot showing the schematic form for the two-band extended s-wave gap at zero temperature, for various values of the DOS parameter, $0.25 < n_1 < 0.5$. (b) Temperature dependence of the rms gap amplitudes on bands one and two, and the overall gap minimum, for the same range of n_1 .

We turn now to the superfluid density, a thermodynamic probe sensitive to the itinerant electronic degrees of freedom, the temperature dependence of which is controlled by the energy dependence of the quasiparticle DOS.⁶¹ The main features of $1/\lambda_L^2$, pointed out above, are its strong temperature dependence across most of the superconducting range, indicating a broad distribution of energy scales in the gap; the upwards curvature of $1/\lambda_L^2(T)$ around $T_c/3$, a hallmark of multiband physics;⁶² and its pronounced flattening at low temperatures, indicating the presence of finite gap minima instead of true nodes.⁶¹ To put these observations on a quantitative footing we have fit the normalized superfluid density, $\rho_s = \lambda_L^2(0)/\lambda_L^2(T)$, to a two-band model similar to that developed by Kogan, Martin and Prozorov (KMP) in Ref. 62. From initial fitting attempts it became apparent that the small energy scale implied by our data could not be captured by a two-band model with isotropic gaps, motivating us to modify the KMP formalism to include gap anisotropy of an extended s-wave form with $\Delta(\phi) \propto (1 + \sqrt{2}\alpha \cos(2\phi))$, as summarized in Methods. In our phenomenological model the gap anisotropy is put in by hand but naturally arises from orbital-dependent effects in microscopic models.⁵⁷ Our fitting parameters are the DOS imbalance between the two bands (parameterized by $n_1 = N_1/N_{\text{total}}$); the coupling constants $\lambda_{11}, \lambda_{22}$ and $\lambda_{12} = \lambda_{21}$, which represent intraband and interband pairing, respectively; the gap anisotropy parameters, α_1 and α_2 ; and a factor γ that controls the relative superfluid weights. Early on in this process we observed that the large-gap band seemed to require little anisotropy, so α_1 was set to zero in the remaining work. Equally good fits to $\rho_s(T)$ are obtained in the range $0.25 < n_1 < 0.5$, with the fit for $n_1 = 0.35$ shown in Fig. 3a. A typical value of the anisotropy pa-

rameter for band 2 is $\alpha_2 = 0.42$. The schematic forms of the energy gaps are shown as functions of angle and temperature in Fig. 3 for $0.25 < n_1 < 0.5$. Note that while there is some variation of Δ_1 and Δ_2 with the choice of n_1 , all fits agree well on the minimum energy gap, $\Delta_{\text{min}}/k_B \approx 0.25 T_c = 2.3$ K, which is a factor of 8 smaller than the large gap in band 1. (Interestingly, very similar conclusions have independently been reached by a field-dependent thermal conductivity study carried out on similar crystals,³⁴ and from penetration-depth experiments,³² where fits to a one-band extended s-wave model estimate $\Delta_{\text{min}}/k_B \approx 0.3 T_c$.) Within our multiband interpretation, the large conductivity peaks seen Fig. 1b are the result of long-lived quasiparticles that are thermally excited in the vicinity of the deep gap minima in band 2. This has two important consequences for the relaxation dynamics: there will be a strong reduction in the phase space for recoil when low energy quasiparticles undergo elastic impurity scattering;^{51,52,58} and Umklapp events,^{49,50} which are necessary if inelastic processes are to relax the electrical current, will require the low energy quasiparticles to partner with quasiparticles on the large-gap band, and these excitations will be strongly gapped.

We emphasize that while the two-band model is used mainly for illustrative purposes, the importance of multiband effects and the presence of finite gap minima — also visible in $R_s(T)$ and $\sigma_1(T)$ — are robust conclusions. In fact, each of the gap values can be directly tied to qualitative features in the temperature dependence of the superfluid density: the gap minimum, Δ_{min} , is fixed by the small range of temperatures over which thermally activated behaviour is observed; Δ_2 , the average value of the gap in the subdominant band, is linked to the upwards curvature in $\rho_s(T)$, which occurs in a range near $T_c/3$;

and the dominant gap, Δ_1 , is set by T_c itself. It is worth mentioning that the factor of 3 ratio between Δ_1 and Δ_2 is difficult to obtain in purely repulsive models of pairing, as the dominant interaction in that case is the interband pairing,⁶² and an unrealistically large imbalance of the density of states ($n_1 \approx 0.05$) must then be assumed to obtain $\Delta_1 \approx 3\Delta_2$.

The observation of activated exponential temperature dependence in our low temperature data and the concomitant identification of finite gap minima are at odds with reports of line nodes in FeSe, in particular the measurements of superfluid density and thermal conductivity in Ref. 30. As pointed out in the introduction, several tunnelling spectroscopy experiments present V-shaped spectra that at first sight appear to be indicative of gap nodes,^{30,35} although the finite-temperature effects (in particular, nonzero conductance at zero bias) that would be expected in the nodal case are not reported. Instead, our observations are in close keeping with the conclusions of a recent thermal conductivity study carried out on the same samples as ours,³⁴ and with heat capacity,²⁸ lower critical field³³ and penetration depth studies.³² While it is tempting to attribute the lifting of accidental gap nodes to impurity scattering,^{32,34} which should homogenize the energy gap in an anisotropic *s*-wave superconductor, we find this hard to reconcile with the exceptionally long quasiparticle mean free path reported here. Nevertheless, sample-to-sample variations of physical properties usually have a microstructural origin. In the case of FeSe, a possible alternative to point-like disorder is the presence of twin boundaries, which form in the nematic phase below 90 K.^{11,12,32,63} These have been shown to have a significant effect on the spatial variation of the energy gap in a recent scanning tunneling spectroscopy experiment.³⁶ Further insights into this may come from local-probe experiments carried out at lower temperatures, if the tunnel junction can be sufficiently cooled, and from measurements on single-domain, macroscopically detwinned samples, when these become available.

Methods

Samples. High quality single crystals of FeSe were grown by vapour transport using the method described in Ref. 19. The sample used for the microwave conductivity experiment was a mm-sized platelet, cleaved from a thicker crystal to have a thickness along the *c* direction of $t = 15 \mu\text{m}$.

Surface impedance and microwave conductivity. Measurements of surface impedance, $Z_s = R_s + iX_s$, were made at two frequencies using cavity perturbation^{64–69} of a self-resonant coil wound from Nb wire and housed inside a Pb:Sn-coated enclosure mounted below the mixing chamber of an MX40 ³He–⁴He dilution refrigerator.³⁸ During the experiments, the resonator was maintained at a fixed temperature of 1.5 K, while the sample temperature was scanned between $T = 0.1$ and 20 K using a silicon hot-finger⁷⁰ thermally linked to the mixing chamber. Data were obtained at 202 MHz using the fundamental mode of the coil resonator, and at 658 MHz using its second overtone. In

both cases, the sample was positioned at a local maximum of the microwave magnetic field, H_{rf} , which was applied parallel to the FeSe layers to induce predominantly in-plane screening currents. Measurements were carried out under conditions of constant H_{rf} , to avoid nonlinearities, and microwave power was kept low enough to prevent self-heating. Temperature-dependent changes in the effective surface impedance, Z_s^{eff} , are obtained directly from shifts in resonator frequency, f_0 , and resonant bandwidth, f_B , using the cavity perturbation approximation $\Delta Z_s^{\text{eff}} = \Gamma (\Delta f_B(T)/2 - i\Delta f_0(T))$. Here Γ is a resonator constant determined empirically from the DC resistivity of FeSe samples from the same batch,³⁴ and Δf_B is the change in resonator bandwidth with and without the sample. Due to the thin sample and low measurement frequencies, finite-size effects are important near and above T_c and are corrected using the 1D finite-size formula $Z_s^{\text{eff}} = Z_s \tanh(i\omega\mu_0 t/2Z_s)$, where Z_s is the surface impedance of a semi-infinite sample. The absolute zero-temperature surface reactance, $X_s(0) = \omega\mu_0\lambda_0$, is set using a previously reported value of the zero-temperature penetration depth, $\lambda_0 = 400 \text{ nm}$.³⁰ The complex microwave conductivity, $\sigma = \sigma_1 - i\sigma_2$, is obtained from the surface impedance using the local electrodynamic relation, $\sigma = i\omega\mu_0/Z_s^*$.

Generalized two-fluid model and modified Drude conductivity. For the purposes of extracting relaxation rate Γ and extrapolating superfluid density to the zero-frequency limit we fit conductivity data to a generalized two-fluid model⁵⁴

$$\sigma = \frac{ne^2}{m^*} \left[\frac{f_s}{i\omega} + \frac{f_n}{\Gamma} \left(\frac{1}{1 + (\omega/\Gamma')^y} - i \text{KK}(\omega/\Gamma', y) \right) \right], \quad (1)$$

where $\Gamma' = \Gamma \times \frac{y}{2} \sin(\frac{\pi}{y})$ is a convenient scaling that makes the integrated quasiparticle spectral weight independent of y . The imaginary part of the quasiparticle conductivity is obtained using a Kramers–Krönig transform⁵⁴ and $f_s + f_n = 1$ in order to conserve spectral weight. Away from the Drude limit ($y = 2$) the frequency exponent y modifies the quasiparticle conductivity to better capture situations with strongly energy-dependent scattering.^{38,53} In FeSe at low temperatures the best-fit value was found to be $y = 1.5$; at high temperatures, where σ_1 has little frequency dependence, the fits are insensitive to the choice of y : the frequency exponent was subsequently fixed at $y = 1.5$ at all temperatures. The static, London superfluid density is $1/\lambda_L^2 = f_s\mu_0 ne^2/m^*$.

Two-band extended *s*-wave superconductor. To model the superfluid density, calculations are made for a clean-limit, two-band superconductor in which the angle dependence of the superconducting order parameter in bands $\nu = 1, 2$ has the form $\Delta_\nu(T)\Omega_\nu(\phi)$, where $\Omega_\nu(\phi) = (1 + \sqrt{2}\alpha_\nu \cos(2\phi)) / \sqrt{1 + \alpha_\nu^2}$ takes an extended *s*-wave form, normalized so that $\langle \Omega_\nu^2(\phi) \rangle_\phi = 1$. Here α_ν controls the degree of gap anisotropy, with gap nodes appearing for $\alpha_\nu \geq 1/\sqrt{2}$. We follow the weak-coupling Eilenberger method described in Ref. 62, modified to incorporate angle-dependent order parameters. Specifically, we solve the self-consistent gap equation

$$\Delta_\nu = \sum_{\mu=1,2} n_\mu \lambda_{\nu\mu} \Delta_\mu \sum_{\omega_n > 0}^{\omega_D} \left\langle \frac{2\pi k_B T \Omega_\mu^2(\phi)}{\sqrt{\Delta_\mu^2 \Omega_\mu^2(\phi) + \hbar^2 \omega_n^2}} \right\rangle_\phi, \quad (2)$$

where the ω_n are the fermionic Matsubara frequencies and the frequency cut-off ω_D is set by the measured T_c . The relative densities of states n_ν and the coupling constants $\lambda_{\nu\mu}$ have the same form as in Ref. 62 and, subject to the constraints $n_1 + n_2 = 1$ and $\lambda_{\nu\mu} = \lambda_{\mu\nu}$, are adjustable parameters. The normalized superfluid density, $\rho_s = \lambda^2(0)/\lambda^2(T)$, is directly computed from $\Delta_1(T)$ and $\Delta_2(T)$ and is a simple linear combination of the contribution from each band: $\rho_s(T) = \gamma\rho_1(T) + (1 - \gamma)\rho_2(T)$, where the parameter γ controls the relative magnitude of the superfluid weights.

- ¹ Sondhi, S., Girvin, S., Carini, J. & Shahar, D. Continuous quantum phase transitions. *Rev. Mod. Phys.* **69**, 315–333 (1997).
- ² Sachdev, S. Quantum criticality: Competing ground states in low dimensions. *Science* **288**, 475–480 (2000).
- ³ Lee, D. & Schofield, A. Correlated quantum fluids and the search for a new theory of metals. *Philos. T. Roy. Soc. A* **358**, 111–125 (2000).
- ⁴ Sachdev, S. Colloquium: Order and quantum phase transitions in the cuprate superconductors. *Rev. Mod. Phys.* **75**, 913–932 (2003).
- ⁵ Coleman, P. & Schofield, A. J. Quantum criticality. *Nature* **433**, 226–229 (2005).
- ⁶ Broun, D. M. What lies beneath the dome? *Nat. Phys.* **4**, 170–172 (2008).
- ⁷ Custers, J. *et al.* The break-up of heavy electrons at a quantum critical point. *Nature* **424**, 524–527 (2003).
- ⁸ Mathur, N. D. *et al.* Magnetically mediated superconductivity in heavy fermion compounds. *Nature* **394**, 39–43 (1998).
- ⁹ von Lohneysen, H. *et al.* Non-Fermi-liquid behavior in a heavy-fermion alloy at a magnetic instability. *Phys. Rev. Lett.* **72**, 3262–3265 (1994).
- ¹⁰ Yeh, A. *et al.* Quantum phase transition in a common metal. *Nature* **419**, 459–462 (2002).
- ¹¹ McQueen, T. M. *et al.* Tetragonal-to-orthorhombic structural phase transition at 90 K in the superconductor Fe_{1.01}Se. *Phys. Rev. Lett.* **103**, 057002 (2009).
- ¹² Watson, M. D. *et al.* Emergence of the nematic electronic state in FeSe. *Phys. Rev. B* **91**, 155106 (2015).
- ¹³ Hsu, F.-C. *et al.* Superconductivity in the PbO-type structure α -FeSe. *Proc. Natl. Acad. Sci.* **105**, 14262–14264 (2008).
- ¹⁴ Medvedev, S. *et al.* Electronic and magnetic phase diagram of β -Fe_{1.01}Se with superconductivity at 36.7 K under pressure. *Nat. Mater.* **8**, 630–633 (2009).
- ¹⁵ Wang, Q.-Y. *et al.* Interface-induced high-temperature superconductivity in single unit-cell FeSe films on SrTiO₃. *Chin. Phys. Lett.* **29**, 037402 (2012).
- ¹⁶ He, S. *et al.* Phase diagram and electronic indication of high-temperature superconductivity at 65K in single-layer FeSe films. *Nat. Mater.* **12**, 605–610 (2013).
- ¹⁷ Ge, J.-F. *et al.* Superconductivity above 100 K in single-layer FeSe films on doped SrTiO₃. *Nat. Mater.* **14**, 285–289 (2014).
- ¹⁸ Peng, R. *et al.* Tuning the band structure and superconductivity in single-layer FeSe by interface engineering. *Nat. Commun.* **5**, 5044 (2014).
- ¹⁹ Böhmer, A. E. *et al.* Lack of coupling between superconductivity and orthorhombic distortion in stoichiometric single-crystalline FeSe. *Phys. Rev. B* **87**, 180505 (2013).
- ²⁰ Chareev, D. *et al.* Single crystal growth and characterization of tetragonal FeSe_{1-x} superconductors. *Cryst. Eng. Comm.* **15**, 1989–1993 (2013).
- ²¹ Imai, T., Ahilan, K., Ning, F. L., McQueen, T. M. & Cava, R. J. Why does undoped FeSe become a high-T_c superconductor under pressure? *Phys. Rev. Lett.* (2009).
- ²² Zhou, Y. & Millis, A. J. Charge transfer and electron-phonon coupling in monolayer FeSe on Nb doped SrTiO₃ (2016). arXiv:1603.02728.
- ²³ Chubukov, A. & Hirschfeld, P. J. Iron-based superconductors, seven years later. *Phys. Today* **68**, 46–52 (2015).
- ²⁴ Zhang, Y. *et al.* Superconducting gap anisotropy in monolayer FeSe thin film (2015). arXiv:1512.06322.
- ²⁵ Mazin, I. I. Superconductivity: The FeSe riddle. *Nat. Mater.* **14**, 755–756 (2015).
- ²⁶ Si, Q., Yu, R. & Abrahams, E. High-temperature superconductivity in iron pnictides and chalcogenides. *Nat. Rev. Mater.* **1**, 16017 (2016).
- ²⁷ Khasanov, R. *et al.* Evolution of two gap behavior of the superconductor FeSe_{1-x}. *Phys. Rev. Lett.* **104**, 087004 (2010).
- ²⁸ Lin, J. Y. *et al.* Coexistence of isotropic and extended s-wave order parameters in FeSe as revealed by low-temperature specific heat. *Phys. Rev. B* **84**, 220507 (2011).
- ²⁹ Lei, H. *et al.* Multiband effects on β -FeSe single crystals. *Phys. Rev. B* **85**, 094515 (2012).
- ³⁰ Kasahara, S. *et al.* Field-induced superconducting phase of FeSe in the BCS-BEC cross-over. *Proc. Natl. Acad. Sci.* **111**, 16309–16313 (2014).
- ³¹ Jiao, L. *et al.* Direct evidence for multi-gap nodeless superconductivity in FeSe (2016). arXiv:1605.01908.
- ³² Teknowijoyo, S. *et al.* Enhancement of T_c by point-like disorder and anisotropic gap in FeSe (2016). arXiv:1605.04170.
- ³³ Abdel-Hafez, M. *et al.* Temperature dependence of lower critical field H_{c1}(T) shows nodeless superconductivity in FeSe. *Phys. Rev. B* **88**, 174512 (2013).
- ³⁴ Bourgeois-Hope, P. *et al.* Thermal conductivity of the iron-based superconductor FeSe: nodeless gap with strong two-band character (2016). arXiv:1603.06917.
- ³⁵ Song, C.-L. *et al.* Direct observation of nodes and twofold symmetry in FeSe superconductor. *Science* **332**, 1410–1413 (2011).
- ³⁶ Watashige, T. *et al.* Evidence for time-reversal symmetry breaking of the superconducting state near twin-boundary interfaces in FeSe revealed by scanning tunneling spectroscopy. *Phys. Rev. X* **5**, 031022 (2015).
- ³⁷ Khasanov, R. *et al.* Evidence of nodeless superconductivity in FeSe_{0.85} from a muon-spin-rotation study of the in-plane magnetic penetration depth. *Phys. Rev. B* **78**, 220510 (2008).
- ³⁸ Truncik, C. J. S. *et al.* Nodal quasiparticle dynamics in the heavy fermion superconductor CeCoIn₅ revealed by precision microwave spectroscopy. *Nat. Commun.* **4** (2013).
- ³⁹ Grimes, C. C., Adams, G. & Bucher, E. Surface-resistance of the heavy-fermion superconductor UPt₃. *Phys. Rev. B* **44**, 4631–4636 (1991).
- ⁴⁰ Bonn, D. A., Dosanjh, P., Liang, R. & Hardy, W. N. Evidence for rapid suppression of quasiparticle scattering below T_c in YBa₂Cu₃O_{7- δ} . *Phys. Rev. Lett.* **68**, 2390–2393 (1992).
- ⁴¹ Kamal, S., Liang, R., Hosseini, A., Bonn, D. & Hardy, W. Magnetic penetration depth and surface resistance in ultrahigh-purity YBa₂Cu₃O_{7- δ} crystals. *Phys. Rev. B* **58**, R8933–R8936 (1998).
- ⁴² Hosseini, A. *et al.* Microwave spectroscopy of thermally excited quasiparticles in YBa₂Cu₃O_{6.99}. *Phys. Rev. B* **60**, 1349–1359 (1999).
- ⁴³ Harris, R. *et al.* Phenomenology of \hat{a} -axis and \hat{b} -axis charge dynamics from microwave spectroscopy of highly ordered YBa₂Cu₃O_{6.50} and YBa₂Cu₃O_{6.993}. *Phys. Rev. B* **74**,

- 104508 (2006).
- ⁴⁴ Hardy, W. N., Bonn, D. A., Morgan, D. C., Liang, R. & Zhang, K. Precision measurements of the temperature dependence of λ in $\text{YBa}_2\text{Cu}_3\text{O}_{6.95}$: strong evidence for nodes in the gap function. *Phys. Rev. Lett.* **70**, 3999–4002 (1993).
 - ⁴⁵ Bonn, D. A. Are high-temperature superconductors exotic? *Nat. Phys.* **1**, 159–168 (2006).
 - ⁴⁶ Nuss, M. C., Mankiewich, P. M., O'Malley, M. L., Westerwick, E. H. & Littlewood, P. B. Dynamic conductivity and “coherence peak” in $\text{YBa}_2\text{Cu}_3\text{O}_7$ superconductors. *Phys. Rev. Lett.* **66**, 3305–3308 (1991).
 - ⁴⁷ Ormeno, R. J., Sibley, A., Gough, C. E., Sebastian, S. & Fisher, I. R. Microwave conductivity and penetration depth in the heavy fermion superconductor CeCoIn_5 . *Phys. Rev. Lett.* **88**, 047005 (2002).
 - ⁴⁸ Milbradt, S. *et al.* In-plane superfluid density and microwave conductivity of the organic superconductor $\kappa\text{-(BEDT-TTF)}_2\text{Cu[N(CN)}_2\text{]Br}$: evidence for d -wave pairing and resilient quasiparticles. *Phys. Rev. B* **88**, 064501 (2013).
 - ⁴⁹ Walker, M. B. & Smith, M. F. Quasiparticle-quasiparticle scattering in high- T_c superconductors. *Phys. Rev. B* **61**, 11285–11288 (2000).
 - ⁵⁰ Duffy, D., Hirschfeld, P. J. & Scalapino, D. J. Quasiparticle lifetimes in a $d_{x^2-y^2}$ superconductor. *Phys. Rev. B* **64**, 224522 (2001).
 - ⁵¹ Hirschfeld, P. J., Putikka, W. O. & Scalapino, D. J. d -wave model for microwave response of high- T_c superconductors. *Phys. Rev. B* **50**, 10250–10264 (1994).
 - ⁵² Schachinger, E. & Carbotte, J. P. Residual absorption at zero temperature in d -wave superconductors. *Phys. Rev. B* **67**, 134509 (2003).
 - ⁵³ Turner, P. J. *et al.* Observation of weak-limit quasiparticle scattering via broadband microwave spectroscopy of a d -wave superconductor. *Phys. Rev. Lett.* **90**, 237005 (2003).
 - ⁵⁴ Özcan, S. *et al.* Electrical transport measurements in the superconducting state of $\text{Bi}_2\text{Sr}_2\text{CaCu}_2\text{O}_{6+\delta}$ and $\text{Tl}_2\text{Ba}_2\text{CuO}_{6+\delta}$. *Phys. Rev. B* **73** (2006).
 - ⁵⁵ Subedi, A., Zhang, L., Singh, D. J. & Du, M. H. Density functional study of FeS, FeSe, and FeTe: Electronic structure, magnetism, phonons, and superconductivity. *Phys. Rev. B* **78**, 134514 (2008).
 - ⁵⁶ Terashima, T. *et al.* Anomalous Fermi surface in FeSe seen by Shubnikov–de Haas oscillation measurements. *Phys. Rev. B* **90**, 144517 (2014).
 - ⁵⁷ Mukherjee, S., Kreisel, A., Hirschfeld, P. J. & Andersen, B. M. Model of electronic structure and superconductivity in orbitally ordered FeSe. *Phys. Rev. Lett.* **115**, 026402 (2015).
 - ⁵⁸ Durst, A. C. & Lee, P. A. Impurity-induced quasiparticle transport and universal-limit Wiedemann-Franz violation in d -wave superconductors. *Phys. Rev. B* **62**, 1270–1290 (2000).
 - ⁵⁹ Zaanen, J. Electrons go with the flow in exotic material systems. *Science* **351**, 1026–1027 (2016).
 - ⁶⁰ Moll, P. J. W., Kushwaha, P., Nandi, N., Schmidt, B. & Mackenzie, A. P. Evidence for hydrodynamic electron flow in PdCoO_2 . *Science* **351**, 1061–1064 (2016).
 - ⁶¹ Prozorov, R. & Giannetta, R. W. Magnetic penetration depth in unconventional superconductors. *Supercond. Sci. Tech.* **19**, R41 (2006).
 - ⁶² Kogan, V. G., Martin, C. & Prozorov, R. Superfluid density and specific heat within a self-consistent scheme for a two-band superconductor. *Phys. Rev. B* **80**, 014507 (2009).
 - ⁶³ Tanatar, M. A. *et al.* Origin of the resistivity anisotropy in the nematic phase of FeSe (2015). arXiv:1511.04757.
 - ⁶⁴ Pippard, A. B. High-frequency resistance of superconductors. *Nature* **158**, 234–235 (1946).
 - ⁶⁵ Altshuler, H. M. Dielectric constant. In *Handbook of microwave measurements II*, 495–548 (Polytechnic Institute of Brooklyn, Brooklyn, NY, 1963).
 - ⁶⁶ Klein, O., Donovan, S. & Dressel, M. Microwave cavity perturbation technique: Part I: Principles. *Int. J. Infrared Milli.* **14**, 2423–2457 (1993).
 - ⁶⁷ Donovan, S., Klein, O., Dressel, M. & Holczer, K. Microwave cavity perturbation technique: Part II: Experimental scheme. *Int. J. Infrared Milli.* **14**, 2459 (1993).
 - ⁶⁸ Huttema, W. A. *et al.* Apparatus for high-resolution microwave spectroscopy in strong magnetic fields. *Rev. Sci. Instrum.* **77**, 023901 (2006).
 - ⁶⁹ Bonn, D. A. & Hardy, W. N. Microwave Electrodynamics of High Temperature Superconductors. In *Handbook of High-Temperature Superconductivity*, 145–214 (Springer, New York, 2007).
 - ⁷⁰ Sridhar, S. & Kennedy, W. L. Novel technique to measure the microwave response of high- T_c superconductors between 4.2 K and 200 K. *Rev. Sci. Instrum.* **59**, 531–536 (1988).

Acknowledgements

We thank A. V. Chubukov, J. S. Dodge, N. Doiron-Leyraud, A. V. Frolov, P. J. Hirschfeld, M. P. Kennett and L. Taillefer for discussions and correspondence. Research support was provided by the Natural Science and Engineering Research Council of Canada, the Canadian Institute for Advanced Research, and the Canadian Foundation for Innovation.

Author contributions

M.L. and D.A.B. carried out the initial measurements of surface resistance and penetration depth. N.L.H. and D.M.B. designed and set up the dilution-refrigerator-based coil-resonator system and carried out the low temperature surface impedance measurements. S.C., R.L., W.N.H. and D.A.B. contributed to the growth of FeSe crystals. D.M.B. and N.L.H. carried out numerical work for the two-band modelling. D.A.B. and D.M.B. wrote the paper. D.A.B., E.G. and D.M.B. supervised the project.

Additional information

Competing financial interests. The authors declare no competing financial interests.

Corresponding author

Correspondence and requests for materials should be addressed to D.M.B. (email: dbroun@sfu.ca).